Check for updates

Hydrogeochemical temporal variations related to the recent volcanic eruption at the Cumbre Vieja Volcano, La Palma, Canary Islands

Cecilia Amonte[1,2]*, Gladys V. Melián[1,2], María Asensio-Ramos[1], Nemesio M. Pérez[1,2], Eleazar Padrón[1,2], Pedro A. Hernández[1,2] and L. D'Auria[1,2]

[1]Instituto Volcanológico de Canarias (INVOLCAN), Santa Cruz de Tenerife, Spain, [2]Instituto Tecnológico y de Energías Renovables (ITER), Santa Cruz de Tenerife, España

From October 2017, as a response to the occurrence of several seismic swarms on La Palma (Canary Islands, Spain), we strengthened the volcano monitoring of the Cumbre Vieja system by carrying out periodic hydrogeochemical sampling at different points of interest. Two galleries—Peña Horeb (PH) and Trasvase Oeste (TO)—and one well—Las Salinas (LS)—were selected with this objective. Significant temporal variations in the pH, EC, ion content (HCO_3^-, F^-, Cl^-, Br^-, SO_4^{2-}, Na^+, Ca^{2+}, and Mg^{2+}), partial pressure of carbon dioxide (pCO_2), and isotopic signature of dissolved CO_2 ($\delta^{13}C\text{-}CO_2$) were observed throughout the study period. These changes were observed in both chemical and isotopic compositions and were related to the interaction between deep volcanic fluids and groundwaters. They coincided with the occurrence of different seismic swarms, leading to the final Tajogaite volcano eruption, which occurred in Cumbre Vieja from 19 September to 13 December 2021. This work highlights the usefulness of monitoring the chemical and isotopic composition of the groundwaters related to active volcanic systems as they can provide important information about the magmatic gas input in the aquifers.

KEYWORDS

Cumbre Vieja eruption, groundwater, hydrogeochemistry, La Palma, Tajogaite volcano, volcanic surveillance

Introduction

Geochemical techniques are widely used in the field of volcanic monitoring. Most studies are based on volcanic gas emissions, with the aim to quantify the gases released into the atmosphere through diffuse soil emission or/and visible emissions such as fumaroles, hot springs, or plume degassing from active craters (Allard et al., 1991; Pérez et al., 1994; Chiodini et al., 1996; Gerlach et al., 2001; Mori et al., 2001; Hernández et al., 2006; Melián et al., 2012; Padrón et al., 2012; Pérez et al., 2013; Padrón et al., 2015;

Inguaggiato et al., 2018; Taran et al., 2018; Alonso et al., 2021; Melián et al., 2021; Padrón et al., 2021). Furthermore, the aquifer is also affected by the ascent of volcanic gases where they could pass through and be trapped or dissolved in it, producing changes in the chemical and/or isotopic composition of groundwaters. For instance, the main soluble volatiles released from magma (SO_2, HCl, HF, and CO_2) can dissolve in water and increase the concentration of characteristic ions present in the groundwaters: SO_4^{2-}, Cl^-, F^-, and HCO_3^- (Armienta et al., 2008). Another factor to consider is that the dissolution of a large volume of acid volcanic gases can increase leaching processes from the solid matrix, which also produces chemical composition changes in groundwaters (Armienta et al., 2008). Therefore, the hydrogeochemical monitoring of groundwaters can provide important information about the internal temporal and spatial changes in heat and gas transfer in a volcanic system (Federico et al., 2002). Literature on this subject contains different works describing how significant variations in the chemical and isotopic composition of groundwaters were detected prior to a volcanic event, providing valuable information about the system being studied (Wakita et al., 1978; King, 1986; Thomas, 1988; Zhang et al., 1995; Hernández et al., 2001; Salazar et al., 2002; Martin-Del Pozzo et al., 2002; Carapezza et al., 2004; Federico et al., 2004; Pérez et al., 2007; Padrón et al., 2008; Melián et al., 2014; Marrero, 2010; Inguaggiato et al., 2018; Amonte et al., 2021; Amonte et al., 2022).

This work is focused on La Palma Island (Canary Archipelago, Spain) which can be divided, from a hydrogeological point of view, into four zones and the Caldera de Taburiente (impermeable base), as shown in Figure 1A (Navarro, 1993). The island is characterized by the existence of a central aquifer (Figure 1A) located on the highest part of the north shield volcano, described as a great erosive unconformity in the shape of a bucket. This structure was called "Coebra" in the Insular Hydrological Plan (Navarro, 1993) and gives rise to the springs and galleries inside Caldera de Taburiente (Bravo & Coello, 1979). The groundwaters from the north part of La Palma are characterized by low mineralization related to high rainfall (75–175 mm; AEMET, 2022) and the presence of an elevated groundwater flow (Benavides, 2019). In contrast, the groundwaters inside Caldera de Taburiente present a higher ion content, which can be attributed to three factors: lithology, rainfall, and geothermal activity (König, 1997). The Cumbre Vieja Volcano has also a high permeability, which favors rainfall infiltration. This permeability is controlled by the presence of vertical dikes which hamper the groundwater circulation from acquiring the water table a stepped profile (Padrón, 2015). Figures 1B,C show the hydrogeological profile of Valle de Aridane (A-A′) and the remaining area of Cumbre Vieja (B-B′), detailing the geological structures of each zone (Navarro, 1993). In addition, the groundwaters from Cumbre Vieja present a high content of dissolved acid volcanic gases, especially CO_2, commonly associated with volcanic zones

(Veeger, 1991). This interaction between groundwater and CO_2 favors weathering reactions, increasing the content of sodium (Na^+), calcium (Ca^{2+}), and magnesium (Mg^{2+}), forming carbonate, bicarbonate, and sulfate salts. This explains why the groundwaters in this zone are characterized as sodium bicarbonate (Na^+-HCO_3^-) type, common in basaltic areas (Custodio, 1986). As explained previously, the Cumbre Vieja volcanic system presents high permeability and, thus, a high groundwater flow. However, during the extraction of groundwater, part of the dissolved CO_2 is released into the atmosphere, the waters become bicarbonate-oversaturated, and precipitating reactions occur. For this reason and because of seawater intrusion due to the proximity to the coast, there are few galleries and wells that can be reliably used as groundwater collection points in Cumbre Vieja.
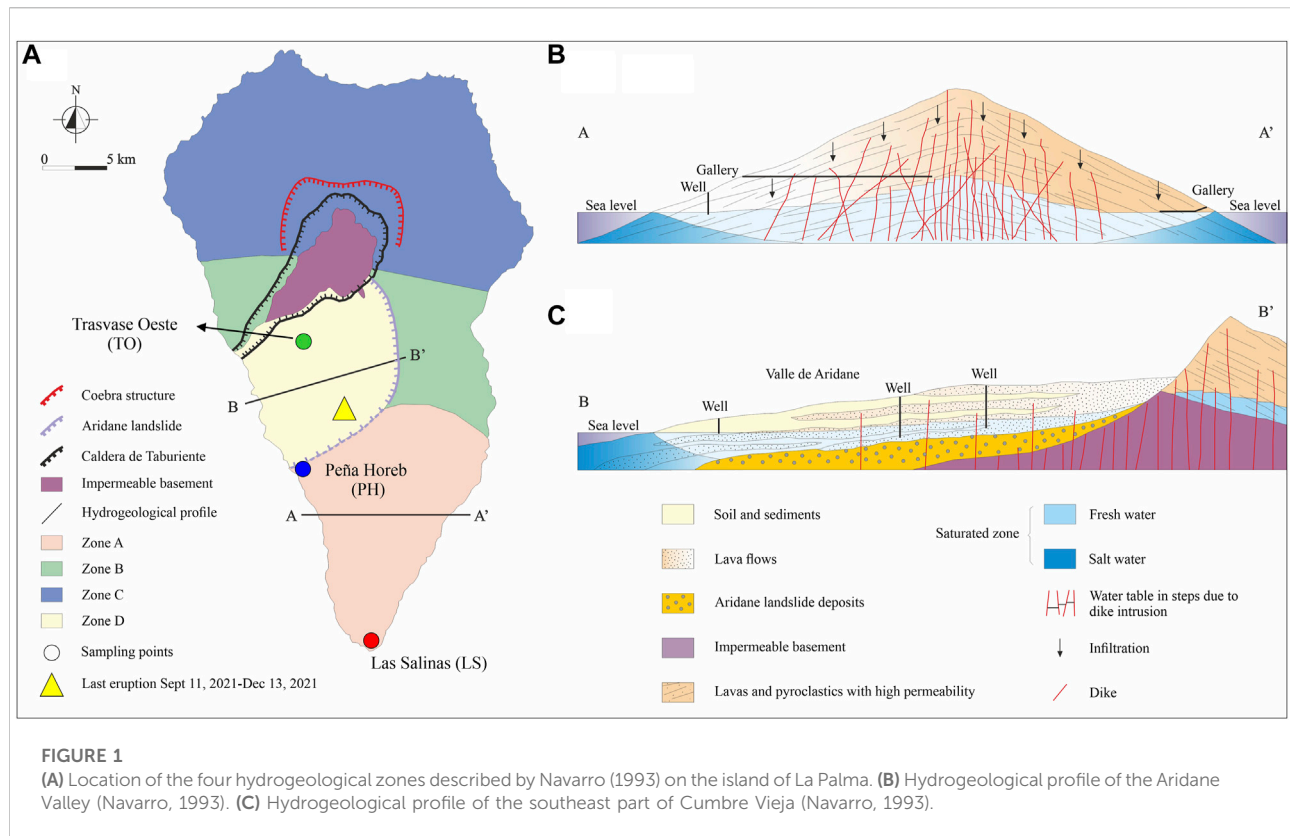
This work is focused on the temporal variation of the chemical and isotopic composition of groundwaters of La Palma and their correlation with the seismic activity and the last eruption which occurred between September and December 2021 at the Cumbre Vieja volcanic system. Three sampling points were selected (Figure 1A): two horizontal wells (galleries)—Peña Horeb (PH) and Trasvase Oeste (TO)—and one well—Las Salinas (LS). According to Navarro (1993), the groundwaters from TO are from the Aridane Valley (zone D, Fig, 1a), while PH and LS are in the west-south and southeast parts of Cumbre Vieja (zone A, Figure 1A).

Geological setting of La Palma

La Palma Island (706 km^2) is located at the northwestern end of the Canary Islands, being the second largest island of the archipelago with the highest elevation (2,423 m asl). The structure of La Palma is constituted by three units: basal complex, older volcanic series, and recent volcanic series making up two principal edifices: one central type in the north (older series, 2.0–0.51 Ma) and a southern N-S ridge (recent series, 0.81 Ma–now) (Staudigel et al., 1986; Ancochea et al., 1994).

The basal complex is constituted by submarine materials and crops out at the bottom of Caldera de Taburiente and Barranco de las Angustias toward the SW. Caldera de Taburiente is a depression of 1,500 m depth located in the central part of the northern edifice, formed by erosive processes (Ancochea et al., 1994). The remains of another volcanic edifice, Cumbre Nueva, can be observed further south. The southern N-S ridge is formed by the Cumbre Nueva series (0.7–0.8 Ma) in its northern part, while the southern part is made up of more recent materials from the so-called Cumbre Vieja series (0–0.5 Ma).

Volcanic activity has been observed in the southern part of the island during the last 125 ka, where the Cumbre Vieja Volcano has been constructed (Figure 1A) (Day et al., 1999). The rift is 20 km long and up to 1,950 m in elevation, covering

FIGURE 1
(A) Location of the four hydrogeological zones described by Navarro (1993) on the island of La Palma. **(B)** Hydrogeological profile of the Aridane Valley (Navarro, 1993). **(C)** Hydrogeological profile of the southeast part of Cumbre Vieja (Navarro, 1993).

220 km^2 with many cinder cones appearing along the crest of this ridge (Padrón et al., 2015). Historical eruptions in the last 500 years (a total of 8) have been associated with eruptive centers in the Cumbre Vieja volcanic ridge with strombolian and phreatic–strombolian behaviors (Ancochea et al., 1994), being the last Tajogaite volcano in 2021.

Cumbre Vieja last eruption

On 19 September 2021, a volcanic eruption started at the SW flank of the Cumbre Vieja Volcano, in the municipality of El Paso (Global Volcanism Program, 2013), about 20 km NW of the place where the last eruption in La Palma occurred (Teneguía Volcano, 1971). The eruption occurred with a large explosion and the opening of two fissures hundreds of meters long, aligned in the NS direction and separated from each other by about 200 m (PEVOLCA, 2022a). The Tajogaite volcanic eruption has been considered by far the most important and devastating urban eruption of the last 100 years in Europe: according to Copernicus European Union's Earth observation program (JRC, 2021), the lava flows covered 12.4 km^2 and affected a total of 3,126 buildings, destroying 2,988 buildings and causing the evacuation of ~7,500 residents. After 85 days of activity, the eruption ended on 13 December 2021.

The first precursory signals of this eruptive process started, after 46 years of seismic silence, with two remarkable seismic swarms beneath the Cumbre Vieja Volcano in 2017 and 2018, respectively, consisting of a sequence of events with depths between 14 and 28 km with a maximum magnitude of 2.7 (D'Auria et al., 2022) (Table 1). Four additional seismic swarms were registered in 2020 and three in 2021 (Table 1). In the following days, the number of earthquakes increased constantly, while ground deformation reached the maximum value (~20 cm), and an increase in the amount of diffuse magmatic gases (CO_2 and H_2S) was detected around the area of Cabeza de Vaca (Santana de León et al., 2022). The eruption started just ~1 week after the beginning of the last seismic swarm. The eruptive style was mainly strombolian, with many explosions which included tephra fall (bombs, lapilli, and ash) from the eruption plumes but also effusive periods with fountain-fed lava flows and partial collapses of the cone (D'Auria et al., 2022; Pankhurst et al., 2022; Romero et al., 2022). The lava flows moved over 5 km west to the sea, and in less than 3 months, a lava field of >12 km^2 with thicknesses of up to tens of meters was formed (4.4 km^2). This eruption was the largest among the seven previous eruptions that have occurred in La Palma in the last 500 years (D'Auria et al., 2022) and the first sub-aerial eruption in the Canary Islands that has been studied in detail. This, together with the unprecedented and detailed way in which this eruption

TABLE 1 List of seismic swarms that occurred during the period October 2017–April 2022 in the La Palma Island.

Date	No. of events	Duration (days)	Maximum magnitude	Released energy (MJ)	Depth (km)
08/10/2017–15/10/2017	26	27	1.2	0.41	20
10/02/2018–15/02/2018	77	103	1.4	4.53	21
24/07/2020–02/08/2020	139	219	1.8	17.9	22
08/10/2020–10/10/2020	98	61	1.3	2.97	28
17/11/2020–19/11/2020	21	29	1.4	1.28	5.2
21/11/2020	13	6	1.2	0.76	27
23/12/2020–26/12/2020	72	29	2.5	53.0	23
31/01/2021–01/02/2021	138	25	1.8	31.7	18
25/06/2021–27/06/2021	32	42	1.7	3.30	24
27/08/2021–27/08/2021	5	6	1.3	0.44	13

was documented (Wadsworth et al., 2022), has made it one of the most important eruptions in recent times.

Methods

Sample collection

Water sampling was carried out in PH (153 samples), TO (214 samples), and LS (329 samples) from October 2017 to April 2022. The sampling frequency varied: during the eruption, the samples were collected daily, while before and after, the samples were collected three times a week. From March to July 2020, sampling was impossible due to the lockdown consequence of the COVID-19 pandemic. In the case of PH, the area where the sampling point is located was affected by very strong gas emissions during the last part of the eruption, and access was forbidden; thus, the last data collected were on 15 November 2021. All the samples were collected and stored in different types of flacons depending on the analysis that would be performed later and analyzed in the geochemical laboratory of INVOLCAN, Canary Island, Spain. Water samples were also collected (40 ml) in a sodium hydroxide solution (NaOH, 10 ml) to determine the total dissolved inorganic carbon (TDIC). In this way, all the inorganic carbon dissolved species are maintained as carbonates to prevent the possible losses of carbon by degassing $CO_{2(g)}$.

Analytical techniques

Water pH and EC were measured in each water sample using a PHM 92 pH-meter (Radiometer, Copenhagen, Denmark) and a CDM210 conductivity meter (Radiometer), respectively. Alkalinity in the regular water samples and the TDIC in the NaOH solution were determined by titration with diluted hydrochloric acid (HCl) using an automatic titration system

(716 DMS Titrino, Metrohm, Herisau, Switzerland). Each sample was analyzed in triplicate obtaining good repeatability with relative standard deviations (RSDs) lower than 1%. In the case of TDIC, the blank NaOH sampling solution was titrated, and the results were subtracted from the results obtained for the samples in NaOH (Marrero, 2010) to avoid the possible contribution of carbon species originally present in the alkaline solution. From the TDIC content, pH values, and water temperature (*in situ* determination), the partial pressure of CO_2 in each sample (expressed in atm) was calculated.

Ion chromatography (IC) was used for cation and anion determinations. Cation concentrations (Na^+, K^+, Ca^{2+}, and Mg^{2+}) were determined in filtered acidified samples using an 861 Advanced Compact IC system coupled with an 838 Advanced IC Sampler Processor (Metrohm). Anion concentrations (F^-, Cl^-, Br^-, and SO_4^{2-}) were determined using a Dionex ICS-2100 system coupled with a Dionex AS-DV autosampler (Thermo Scientific, Massachusetts, United States). In both cases, conductivity detection was used. More details about the IC conditions can be found in the study by Amonte et al. (2021). To control the quality of the whole ion analysis, the ion balance error—IBE = (sum of cations–sum of anions)/(sum of cations + sum of anions)—was calculated for each sample, discarding the results of those whose IBE was greater than ±5%.

Dissolved CO_2 carbon isotope (δ^{13}C-CO_2) analyses were conducted after equilibration with a host gas (helium in this case) and extraction, following the methodology described by Capasso and Inguaggiato (1998). Analyses were conducted using a Thermo Finnigan MAT 253 isotope ratio mass spectrometer (IRMS). The results are reported in δ units per mil versus Vienna Pee Dee Belemnite standard (VPDB) with a precision of ± 0.2‰ for δ^{13}C-CO_2.

The Sinclair probability plot technique was applied to the anion content (HCO_3^-, F^-, Cl^-, Br^-, and SO_4^{2-}), the pCO_2, and the isotopic signature of dissolved CO_2 (δ^{13}C-CO_2) to distinguish different sources of geochemical data (Sinclair, 1974). This technique

TABLE 2 Statistical summary of pH, EC, water temperature (T), alkalinity (HCO₃), partial pressure of CO₂ (pCO₂), ion content (F⁻, Cl⁻, Br⁻, SO₄²⁻, Na⁺, K⁺, Ca²⁺, and Mg²⁺), and carbon isotopic signature in dissolved CO₂ (δ¹³C-CO₂) for Peña Horeb (PH), Trasvase Oeste (TO), and Las Salinas (LS) groundwater samples.

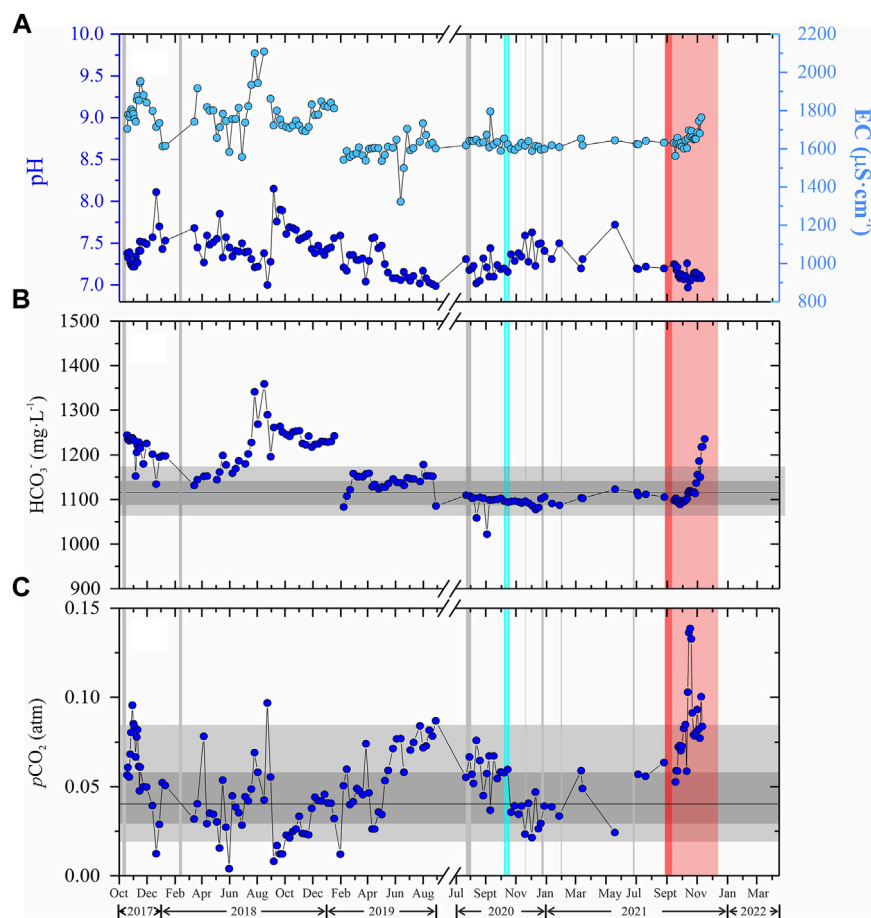|		pH	EC ($\mu S \cdot cm^{-1}$)	T (°C)	HCO_3^- ($mg \cdot L^{-1}$)	pCO_2 (atm)	F^- ($mg \cdot L^{-1}$)	Cl^- ($mg \cdot L^{-1}$)	Br^- ($mg \cdot L^{-1}$)	SO_4^{2-} ($mg \cdot L^{-1}$)	Na^+ ($mg \cdot L^{-1}$)	K^+ ($mg \cdot L^{-1}$)	Ca^{2+} ($mg \cdot L^{-1}$)	Mg^{2+} ($mg \cdot L^{-1}$)	$\delta^{13}C\text{-}CO_2$ (‰ vs. VPDB)
PH	Min.	7.0	1,080	18	977	3.9×10^{-3}	0.55	61	0.10	38	152	63	50	78	−11.7
	Max.	8.4	2,220	24	1,359	1.4×10^{-1}	1.06	177	0.80	75	233	160	105	163	−1.14
	Mean	7.3	1,692	30	1,156	5.4×10^{-2}	0.76	95	0.28	55	184	85	61	117	−8.11
TO	Min.	6.3	334	17	239	1.9×10^{-2}	0.25	10	0.02	3.4	40	10	17	17	−12.6
	Max.	7.4	468	25	339	2.4×10^{-1}	0.45	21	0.07	8.6	53	14	26	28	−6.15
	Mean	6.8	426	20	266	8.1×10^{-2}	0.34	13	0.04	4.9	43	11	19	21	−10.9
LS	Min.	6.1	23,720	19	343	1.5×10^{-2}	n.d.	14,183	37	1,978	9,483	300	359	959	−12.4
	Max.	7.5	47,300	24	716	4.0×10^{-1}	n.d.	23,640	74	8,455	12,820	526	1,199	1,541	1.93
	Mean	6.5	41,654	22	529	1.1×10^{-1}	n.d.	18,858	62	2,552	10,774	400	429	1,288	−4.68

n.d.: no data.

FIGURE 2
Temporal evolution of **(A)** pH and EC (μS·cm^{-1}), **(B)** alkalinity (HCO$_3^-$, mg·L^{-1}) and **(C)** partial pressure of CO$_2$ (pCO$_2$, atm) of groundwater from Peña Horeb (PH). The background mean population (black lines) and standard deviation values ($\pm$1σ and $\pm$2σ) are shown as thick grey lines. Seismic swarms are shown as vertical solid grey lines, and the long period event as a turquoise line. The pre-eruptive seismicity is shown as red band while the eruptive period is represented as lightly red band.

consists of plotting the logarithm of the data versus the cumulative frequency percentage on a probability scale. The result is a bimodal distribution, two log-normal population plots as an S-type curve, where the inflection point of the curve allows distinguishing the threshold value between both populations.

Results and discussion

pH, EC, cation (Na$^+$, K$^+$, Ca^{2+}, and Mg^{2+}) and anion (HCO$_3^-$, F$^-$, Cl$^-$, Br$^-$, and SO$_4^{2-}$) concentrations, pCO$_2$, and δ^{13}C-CO$_2$ in the groundwater from PH, TO, and LS are summarized in Table 2 (for complete data, see Supplementary Tables A1–A3). Figures 2–4 show the temporal variations of pH, EC, HCO$_3^-$, and pCO$_2$ for PH, TO, and LS.

The Sinclair probability plots for the studied parameters are shown in Figures ESM1, ESM2, ESM3, ESM4, and ESM5 of the Supplementary Material. In all of them, two log-normal populations (background and peak) can be distinguished. Table 3 summarizes the mean of background and peak populations, as well as the standard deviation values. To construct the temporal evolutions of each parameter, the mean value of the background population and the standard deviation values, plus one and two standard deviations ($\pm$1σ and $\pm$2σ), provided by the Sinclair plot, were represented as gray bands. In all the plots, the seismic swarms (vertical gray lines), long-period event (vertical turquoise line), pre-eruption seismicity (vertical red band), and the eruptive period (vertical light red band) are also shown.
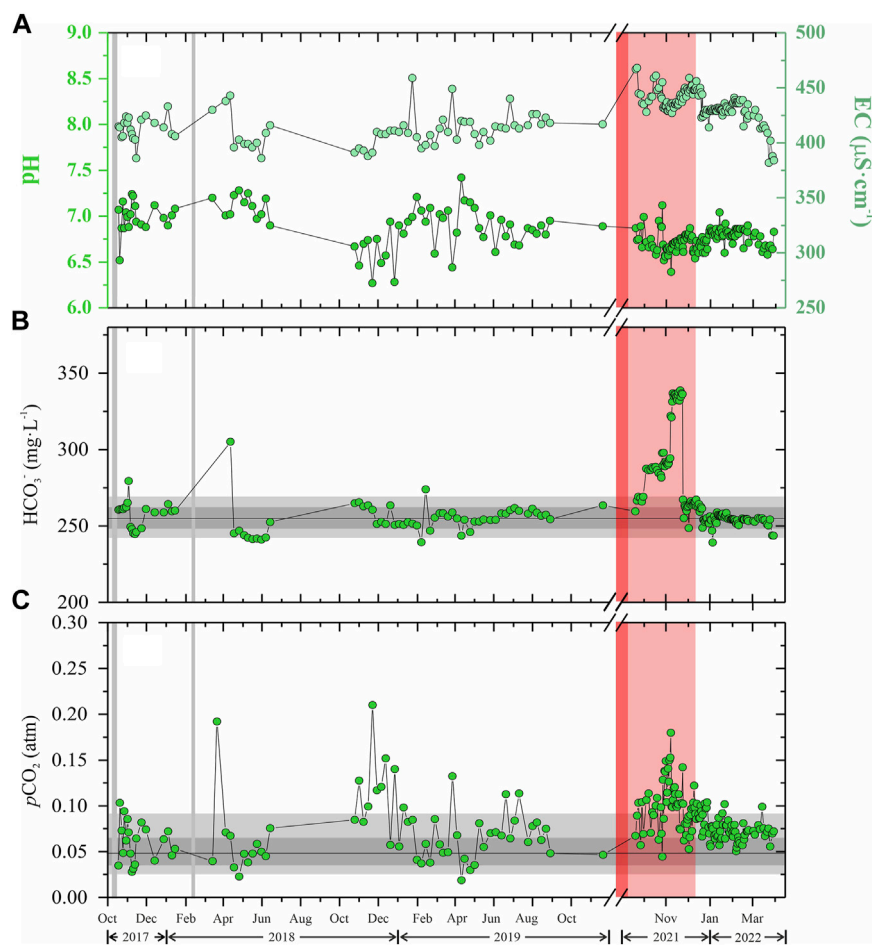
FIGURE 3
Temporal evolution of **(A)** pH and EC (μS·cm^{-1}), **(B)** alkalinity (HCO$_3^-$, mg·L^{-1}) and **(C)** partial pressure of CO$_2$ (pCO$_2$, atm) of groundwater from Trasvase Oeste (TO). The background mean population (black lines) and standard deviation values ($\pm 1\sigma$ and $\pm 2\sigma$) are shown as thick grey lines. Seismic swarms are shown as vertical solid grey lines, and the long period event as a turquoise line. The pre-eruptive seismicity is shown as red band while the eruptive period is represented as lightly red band.

Study of the pH and EC variations

The mean values measured for the groundwater pH were 7.4, 6.8, and 6.5 for PH, TO, and LS, respectively. As can be seen in the figures, there are some periods where the pH values show variations. PH exhibits a progressive decrease from February 2018 to August 2019, while the same trend is observed from February 2018 to April 2019 for LS (Figures 2A, 4A). In the case of TO, the pH values show a slight decrease during the eruptive period. Thermal waters at Stromboli (Italy) also showed a clear decrease in the pH before a violent explosive paroxysm in 2003, which was associated with a direct increase in the input of acid gases, especially CO$_2$ (Carapezza et al., 2004). Thus, a decrease in the pH values in the groundwaters is directly related to an

increase in the amount of CO$_2$ being dissolved. In fact, very low additions of CO$_2$ have a higher impact on pH than other acid volcanic gases, such as H$_2$S (Federico et al., 2004). Regarding the EC values, mean values of 1,692, 426, and 41,654 μS cm^{-1} were measured for PH, TO, and LS, respectively. There are two considerable increases in this parameter: after the February 2018 seismic swarm and during the eruptive period. These changes are more evident in PH than in TO and LS (Figures 2A, 3A, 4A). An increase in EC can be explained as an increase of dissolved ion species, which is a consequence of a stronger water–rock–gas interaction. On the other hand, the highest values of EC are measured in LS, which present values typical for seawater (30,000–60,000 μS cm^{-1}, Zheng et al., 2018). This fact suggests a strong seawater intrusion for being a coastal well.

FIGURE 4
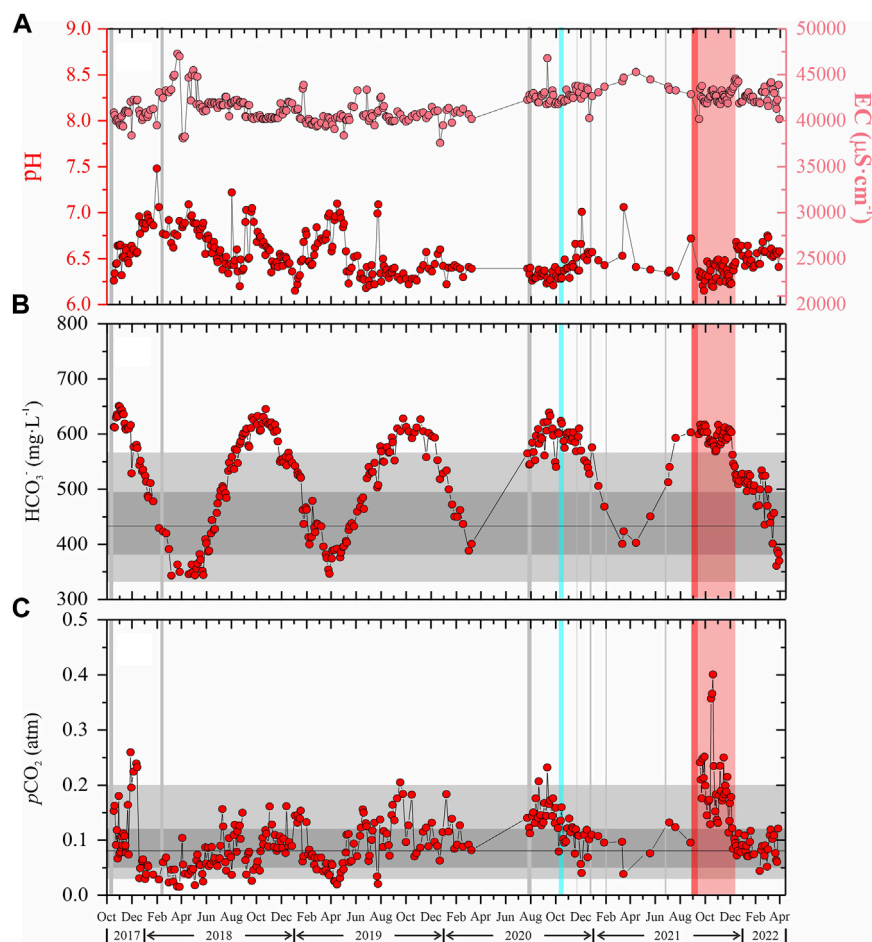Temporal evolution of **(A)** pH and EC ($\mu S \cdot cm^{-1}$), **(B)** alkalinity (HCO_3^-, $mg \cdot L^{-1}$) and **(C)** partial pressure of CO_2 (pCO_2, atm) of groundwater from Las Salinas (LS). The background mean population (black lines) and standard deviation values ($\pm 1\sigma$ and $\pm 2\sigma$) are shown as thick grey lines. Seismic swarms are shown as vertical solid grey lines, and the long period event as a turquoise line. The pre-eruptive seismicity is shown as red band while the eruptive period is represented as lightly red band.

Study of alkalinity (HCO_3^- content)

Another important parameter is alkalinity, expressed as bicarbonate (HCO_3^-) content (Figures 2B, 3B, 4B), since it can provide information about changes in the dissolved CO_2 in the volcanic system. The mean values obtained were 1,156, 266, and 529 mg L^{-1} of HCO_3^- for PH, TO, and LS, respectively. Figures 3B, 4B show, once more, two periods where this parameter was higher than two times the standard deviation of the background population ($+2\sigma$). One occurred after the February 2018 seismic swarm and the other during the eruptive period. Both cases seem to involve large gas emissions, one portion being trapped or dissolved in the aquifer and another released into the atmosphere (Allard et al., 1997; Chiodini et al., 1999). The first change, after the February 2018 seismic swarm, is related to processes of magma ascent from the upper mantle that

perturbed the magmatic reservoir (Santana de León et al., 2022). Because of this, hydrothermal volcanic gases (mainly CO_2) were released. These changes coincide in time with the decrease in the water pH for PH and TO (Figures 2A,B), confirming an increase in the dissolved CO_2 content. A similar behavior was observed in thermal waters from Stromboli (Italy), in which the first anomalies, related to an increase of dissolved CO_2, appeared some months before the December 2002 eruption (Carapezza et al., 2004). The second increase in HCO_3^- was observed during the eruptive period, when large quantities of gases were being emitted (Santana de León et al., 2022; Pardo et al., 2002; Melián et al., 2022; Hayer et al., 2022; PEVOLCA, 2022b). These changes observed in the alkalinity for PH and TO are correlated and supported by the progressive increase of diffuse CO_2 emission measured around the Cumbre Vieja Volcano during 2016–2022 (Santana de León et al., 2022). The maximum HCO_3^- content

TABLE 3 Statistical summary of the results of the probability plot technique for each sampling point dataset.

Sampling point	Geochemical parameter	Background population		Peak population	
		Average	Percentage of the data (%)	Average	Percentage of the data (%)
PH	HCO_3^- (mg·L^{-1})	1,116	62	1,300	3
	pCO_2 (atm)	0.04	75	0.1	7
	F^- (mg·L^{-1})	0.69	60	0.92	8
	Cl^- (mg·L^{-1})	76	42	121	26
	Br^- (mg·L^{-1})	0.21	46	0.52	4
	SO_4^{2-} (mg·L^{-1})	51	46	67	6
TO	HCO_3^- (mg·L^{-1})	255	75	336	6
	pCO_2 (atm)	0.05	22	0.12	17
	F^- (mg·L^{-1})	0.33	88	0.38	6
	Cl^- (mg·L^{-1})	13	74	20	3
	Br^- (mg·L^{-1})	0.04	68	0.07	2.5
	SO_4^{2-} (mg·L^{-1})	4.6	91	8.3	4
LS	HCO_3^- (mg·L^{-1})	435	36	644	3
	pCO_2 (atm)	0.08	79	0.29	2
	Cl^- (mg·L^{-1})	18,817	98	20,612	2
	Br^- (mg·L^{-1})	59	46	70	5
	SO_4^{2-} (mg·L^{-1})	2,476	63	2,687	14

value for PH and TO was registered during the eruptive period, coinciding with the maximum value of the diffuse CO_2 emission (4,435 t d^{-1}), recorded on 14 December 2021 (Santana de León et al., 2022), just the day the eruption ended.

In addition, the existence of different geochemical populations observed in the statistical-graphical study suggests that there have been additional contributions of CO_2 to the waters during the study period. In the case of the LS sampling site (Figure 4B), the temporal evolution of HCO_3^- shows a periodic cycle related to seasonal influence. These variations could be linked to trends in evaporation, the lack of precipitations, and the major role played by underground waters richer than surface waters in solutes (Naselli et al., 2003). These factors make it very difficult to relate the changes in the HCO_3^- content with the volcanic activity.

Study of the partial pressure of CO_2 (pCO_2)

The partial pressure of CO_2 is a geochemical parameter directly linked with the amount of CO_2 dissolved in the groundwaters. In this study, mean values of 5.4×10^{-2}, 8.1×10^{-2}, and 1.1×10^{-1} atm were obtained for PH, TO, and LS groundwaters, respectively (Figures 2C, 3C, 4C). In general, the

samples exhibit values of 1–3 orders of magnitude higher than those expected for waters in equilibrium with the atmosphere (pCO_2 = 2.5×10^{-4} atm; Bellia et al., 2015). PH, TO, and LS groundwaters show two periods where the values of pCO_2 are higher than the standard deviation (+1σ) or even higher than two times the standard deviation (+2σ) of the background population: one after the occurrence of the February 2018 seismic swarm and another during the eruptive period. For PH, the progressive increase of pCO_2 from February 2018 to August 2019 is notorious, which coincides with the decrease in pH and the increase in the HCO_3^- content. TO shows an increase in the pCO_2 values during February–November 2018, while the HCO_3^- content increases. In the case of LS, a progressive increase in pCO_2 values was observed from February to December 2018, but it is less pronounced than in the galleries. The second change is produced during the eruptive period, where the three sampling points exhibit the maximum values of pCO_2 reached during the study period. Increases in the pCO_2 values are directly related to changes in the CO_2 input. These anomalies found in the pCO_2 values of PH, TO, and LS could be attributed to the release of CO_2 by fresh magma that intruded into the volcano plumbing system (Bellia et al., 2015). This behavior was also observed in a thermal well located on the NE side of Stromboli (Stromboli village, Italy), in which the pCO_2 values increased by one order of magnitude,
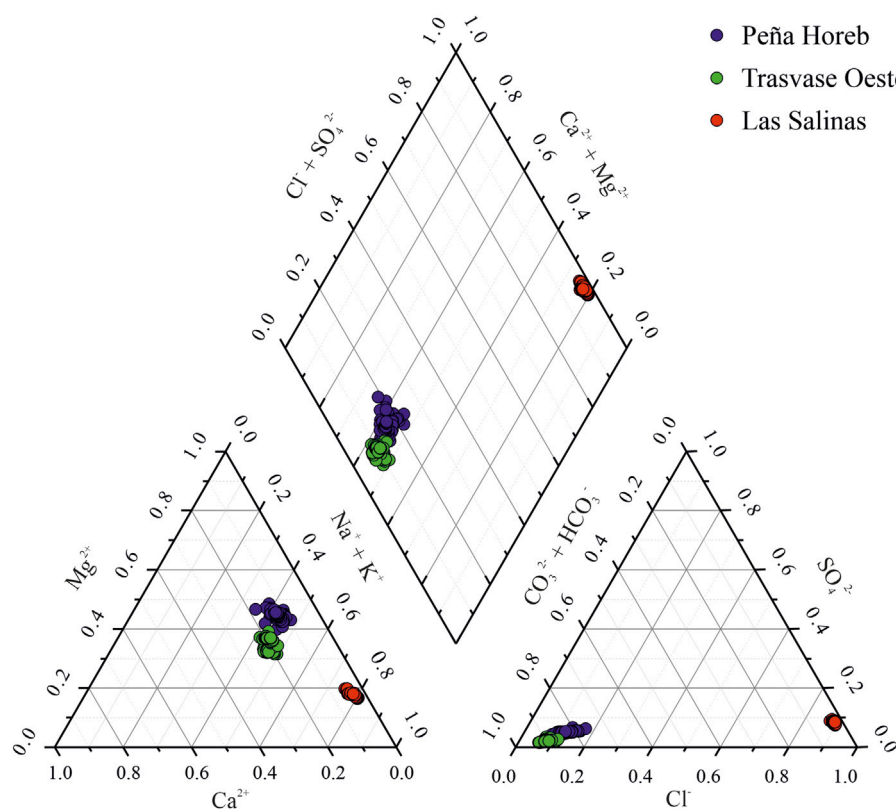
FIGURE 5
Piper diagram where the ion composition of groundwater from Peña Horeb (PH), Trasvase Oeste (TO), and Las Salinas (LS) is represented.

months before the eruption occurred in December 2002 (Inguaggiato et al., 2011). These anomalies were indicative of overpressure of volatile degassing from a new magma-rich batch that interacted with the basal hydrothermal reservoir (Inguaggiato et al., 2011). In addition, the correlation between pH, EC, and HCO_3^- content and the pCO_2 of PH, TO, and LS confirms, once again, the arrival and dissolution of CO_2 into the shallow aquifer.

Study of anions and cations (Na⁺, K⁺, Mg²⁺, Ca²⁺, HCO₃⁻, F⁻, Cl⁻, Br⁻, and SO₄²⁻)

A Piper diagram was constructed from the content of each water sample (Figure 5) to characterize the groundwater's hydrochemical phases. PH, TO, and LS are characterized by a cation content that decreased in abundance as follows: $Na^+ + K^+ > Mg^{2+} > Ca^{2+}$, being plotted in the alkaline element ($Na^+ + K^+$) field (Figure 5). Regarding anion concentrations, HCO_3^- is the dominant anion for PH and TO, followed by Cl^- and SO_4^{2-}. In the case of LS, Cl^- is the major anion followed by HCO_3^- and SO_4^{2-}. The dominance of Cl^- over the other anions in LS provides evidence, once again, of a seawater intrusion in this coastal well.

In summary, waters from PH and TO galleries are exclusively of the sodium bicarbonate ($Na-HCO_3$) type, while LS shows a sodium chloride ($Na-Cl$) water type.

The temporal evolutions of the anion content (F^-, Cl^-, Br^-, and SO_4^{2-}) in the groundwaters from PH, TO, and LS are given in Figures 6–8. The main source of F^- in groundwaters is volcanic activity, which releases magmatic F^- generally as hydrofluoric acid ($HF_{(g)}$) through volcanic degassing (D'Alessandro et al., 2006). For PH groundwater, an interesting progressive increase of the F^- content is observed, starting in August 2018 and reaching the maximum value during the eruption (Figure 6A). This anion in TO groundwater shows stable behavior (Figure 7A), while for LS, its determination was impossible by IC due to the high Cl^- content. A possible explanation for the different comportments of the F^- content for PH and TO is the proximity of the sampling point to the eruptive zone. The presence of F^- in groundwaters is mainly by persistent open conduit degassing (D'Alessandro et al., 2006), and PH is located closer to the eruptive area than TO (Figure 1). Another important source of F^- are volcanic rocks, which are enriched in this anion because HF exsolves partially during the eruptive activity (D'Alessandro et al., 2006). Burton et al. (2003) estimated that just 20% of HF was exsolved from Etnean magma during effusive
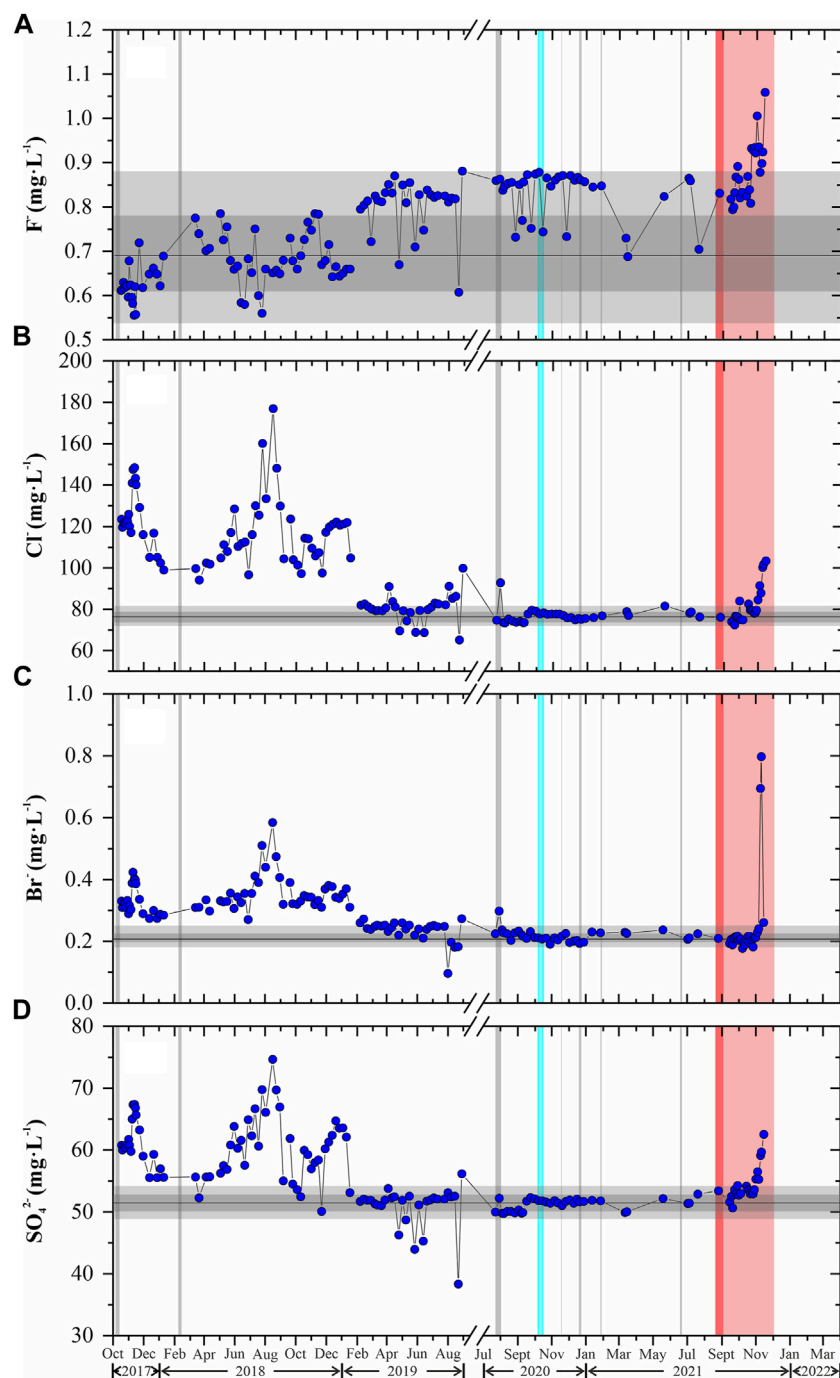
FIGURE 6
Temporal evolution of **(A)** fluoride (F⁻), **(B)** chloride (Cl⁻), **(C)** bromide (Br⁻), and **(D)** sulfate (SO₄²⁻) contents of groundwater from Peña Horeb (PH). The background mean population (black lines) and standard deviation values (±1σ and ±2σ) are shown as thick gray lines. Seismic swarms are shown as vertical solid gray lines, and the long period event is shown as a turquoise line. The pre-eruptive seismicity is shown as a red band, while the eruptive period is represented by a light red band.

activity. It is also worth mentioning that, during explosive activity, big quantities of HF can be adsorbed on the volcanic ash surface, producing a deposition of F⁻ around the volcano even at long distances. This F⁻ may reach the groundwater zone along with percolating rainwater (D'Alessandro et al., 2006). Ash leachate analysis was performed by Rodríguez et al. (2022) who reported a mean value of 261 mg kg⁻¹ of F⁻ in the samples collected during the Tajogaite eruption. These F⁻ contents are
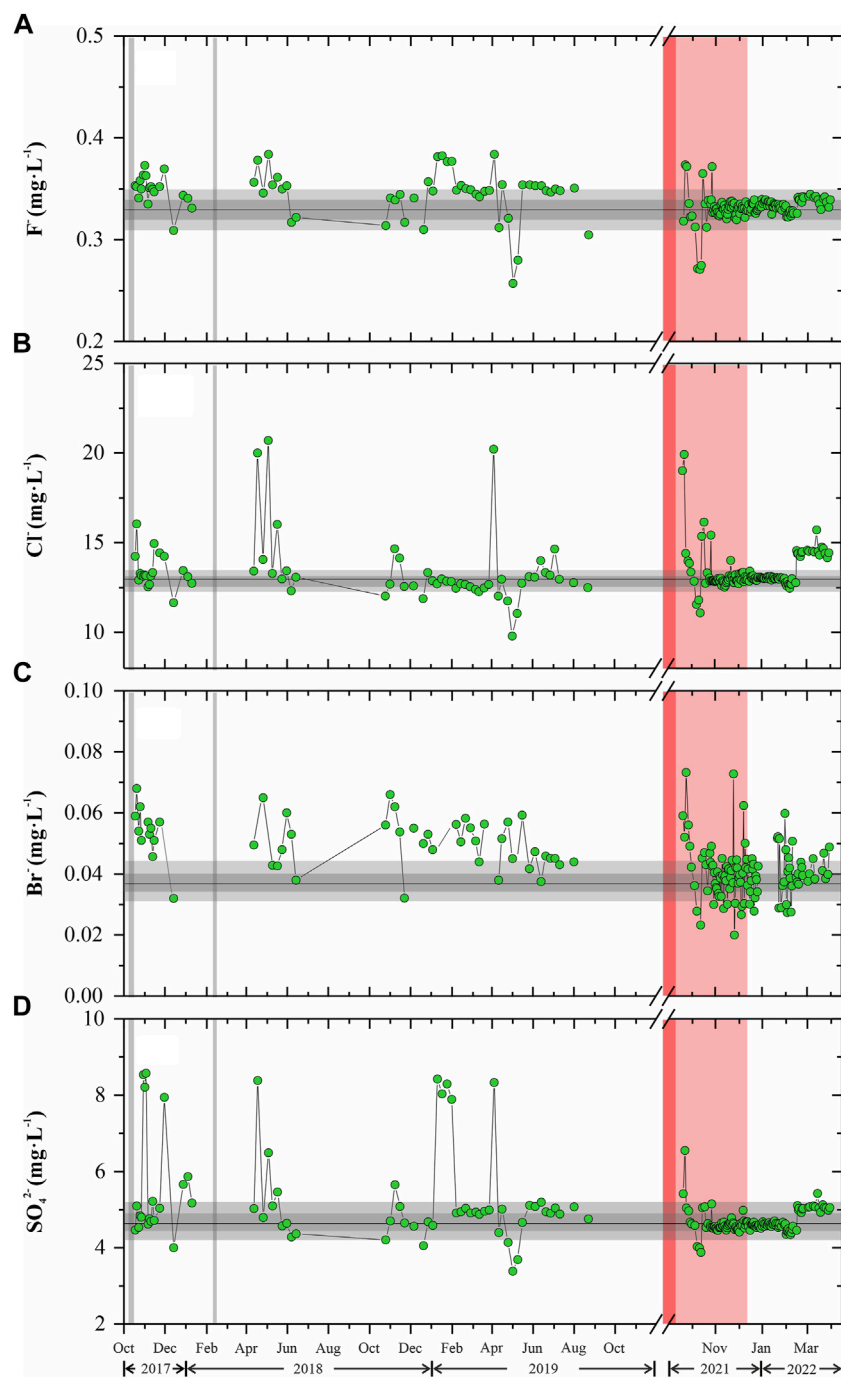
FIGURE 7
Temporal evolution of **(A)** fluoride (F⁻), **(B)** chloride (Cl⁻), **(C)** bromide (Br⁻), and **(D)** sulfate (SO₄²⁻) contents of groundwater from Trasvase Oeste (TO). The background mean population (black lines) and standard deviation values ($\pm1\sigma$ and $\pm2\sigma$) are shown as thick gray lines. Seismic swarms are shown as vertical solid gray lines, and the long period event is shown as a turquoise line. The pre-eruptive seismicity is shown as a red band, while the eruptive period is represented by a light red band.

relatively higher than those observed in other eruptions in the world. For example, D'Addabbo et al. (2006), (2015) presented results of ash leaching samples from Etna (Italy) and Popocatépetl (Mexico) volcanoes, obtaining an F⁻ content

below 100 mg kg⁻¹ from the samples collected in 2012. In La Palma groundwaters, the effect of F⁻ dragging from the ash by the rains will possibly be observed soon, depending on the rainfall regime.
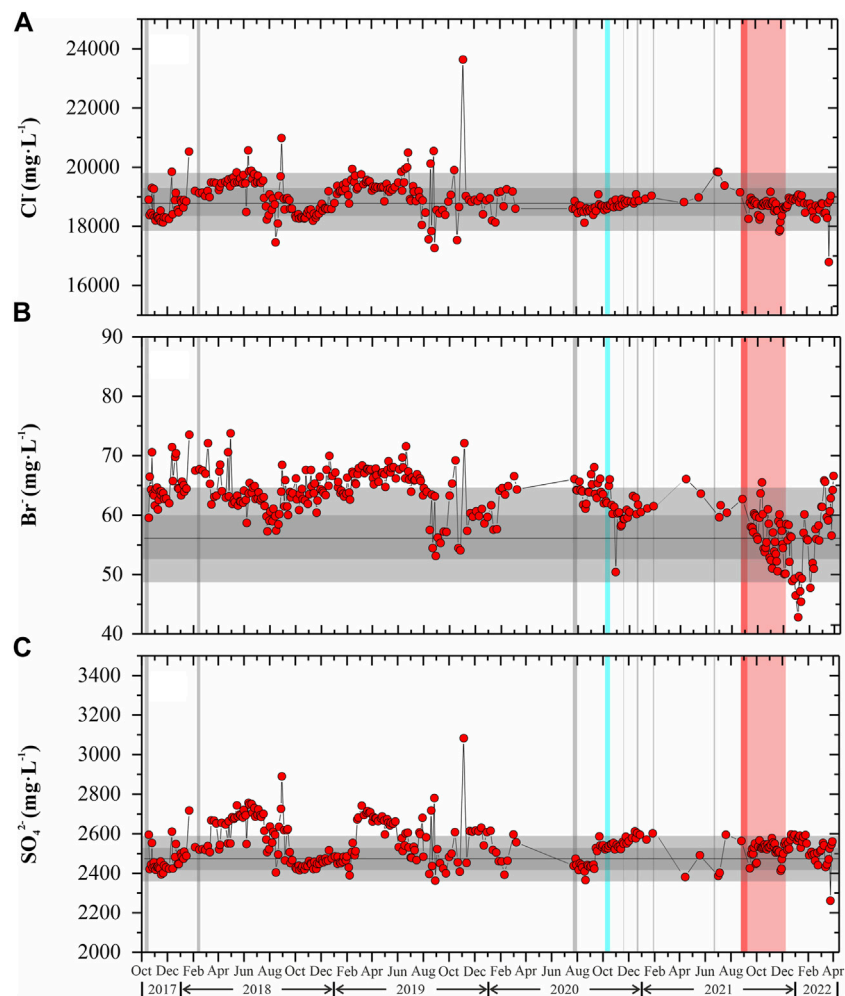
FIGURE 8
Temporal evolution of **(A)** chloride (Cl⁻), **(B)** bromide (Br⁻), and **(C)** sulfate (SO₄²⁻) contents of groundwater from Las Salinas (LS). The background mean population (black lines) and standard deviation values (±1σ and ±2σ) are shown as thick gray lines. Seismic swarms are shown as vertical solid gray lines, and the long period event is shown as a turquoise line. The pre-eruptive seismicity is shown as a red band, while the eruptive period is represented by a light red band.

On the other hand, Cl⁻, Br⁻, and SO₄²⁻ temporal variations showed an increase between April and September 2018, reaching maximum values during the eruptive period for PH and TO (Figures 6, 7). The changes observed for TO groundwater are slighter than those from PH, probably due to the greater proximity of PH to the area where the eruption occurred. Cl⁻ and Br⁻ are tracers close to the ideal conservative behavior due to their hydrophilic characteristic and small ionic size (Alcalá and Custodio, 2008). The most likely source of them in the aquifer is by the dissolution of volatile halides, i.e., HCl and HBr, from the volcanic system (Aiuppa et al., 2005). Martin-Del Pozzo et al. (2002) found an increase in the Cl⁻ content before the Popocatepetl (1994–2000) eruption (Mexico) in some springs, which could be related to HCl from the ascending magma and sublimate remobilization. Regarding SO₄²⁻, its presence is related

to the contribution of sulfur volcanic gases such as H₂S and/or SO₂, which oxidize and dissolve in the aquifer (Marrero, 2010). These endogenous emissions of sulfurous gases occur in spatially defined areas and the vicinity of historic and recent eruptive centers (Marrero, 2010). This may explain why in PH the SO₄²⁻ concentration is higher than that in the TO gallery. For LS groundwater, no trends are observed in the temporal evolution of the anion content. In addition, the increase in Cl⁻ and SO₄²⁻ contents at PH, TO, and LS was related to decreasing pH values, indicative of the interaction between groundwater and magmatic gases, as described at Vulcano in Italy (Capasso et al., 1999). The increase of Cl⁻ and SO₄²⁻ is a result of sublimate remobilization aided by acid magmatic components mixing with the large water system prior to magmatic eruptions (Martin-Del Pozzo et al., 2002). To rule
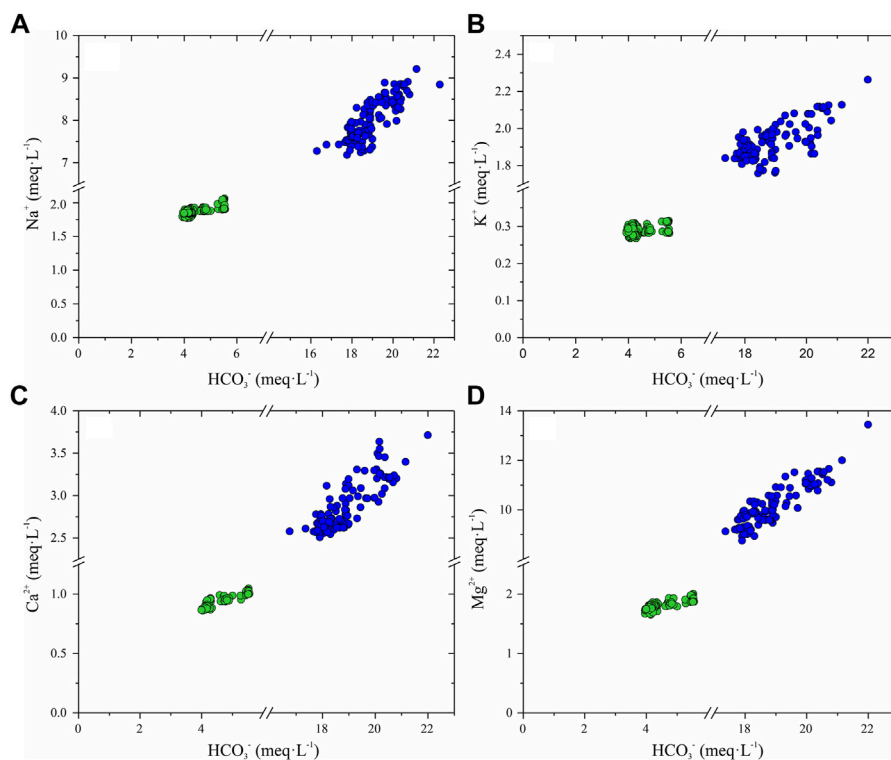
FIGURE 9
Binary diagram of **(A)** sodium (Na$^+$), **(B)** potassium (K$^+$), **(C)** calcium (Ca^{2+}), and **(D)** magnesium (Mg^{2+}) vs. the bicarbonate content (HCO$_3^-$) of groundwaters from Peña Horeb (PH, blue solid circles) and Trasvase Oeste (TO, green solid circles).
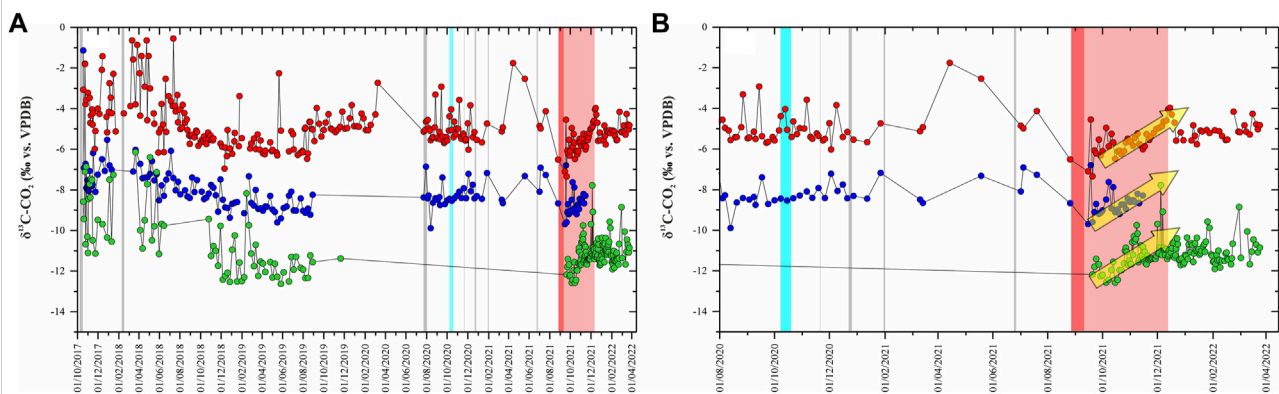

FIGURE 10
Temporal evolution of δ^{13}C-CO$_2$ from groundwaters of Peña Horeb (PH, blue solid circles), Trasvase Oeste (TO, green solid circles), and Las Salinas (LS, red solid circles). **(A)** October 2017 to April 2022. **(B)** From August 2020 to April 2022. Seismic swarms are shown as vertical solid gray lines, and the long period event is shown as a turquoise line. The pre-eruptive seismicity is shown as a red band, while the eruptive period is represented by a light red band.

out that these changes could have been produced by seawater intrusion, Cl$^-$/HCO$_3^-$, SO$_4^{2-}$/Cl$^-$, and Cl$^-$/Br$^-$ mass ratios were calculated for PH, TO, and LS groundwaters. The typical values for seawater are 20–50, 0.12, and 655 for Cl$^-$/HCO$_3^-$, SO$_4^{2-}$/Cl$^-$, and Cl$^-$/Br$^-$ mass ratios, respectively (Alcalá and Custodio, 2008). The average values for Cl$^-$/HCO$_3^-$, SO$_4^{2-}$/Cl$^-$, and Cl$^-$/Br$^-$ mass ratios were 0.08, 0.6, and 352 for PH and 0.04, 0.4, and 396 for TO, respectively. The low values of Cl$^-$/HCO$_3^-$ mass ratio

evidence, once more, the high amount of CO_2 which is dissolved in the aquifer. Both galleries show values of SO_4^{2-}/Cl^- slightly higher than the seawater ratio, showing the addition of sulfur volcanic gases. On the contrary, the mass ratio averages for LS were 37, 0.14, and 307 for Cl^-/HCO_3^-, SO_4^{2-}/Cl^-, and Cl^-/Br^-, respectively. Once again, the high grade of marine intrusion of this coastal well can be appreciated. Cl^-/Br^- mass ratios are very similar for the three sampling points and comparable to those of seawater, meaning that Cl^- and Br^- can be considered a mixture of seawater and volcanic-originated fluids (Rouwet et al., 2009).

To support the chemical changes observed, Figure 9 was constructed, in which cation (Na^+, K^+, Ca^{2+}, and Mg^{2+}) concentrations were plotted *versus* the HCO_3^- content. The input of deep CO_2 makes the groundwater highly reactive to the chemical weathering of the host basaltic rocks (Bellia et al., 2015). As a result of this process, HCO_3^- increases, while Na^+, K^+, Ca^{2+}, and Mg^{2+} are released into the solution. Figure 8 shows the positive correlation between HCO_3^- and these cations for PH and TO. In the case of LS, there is no correlation between the cation content and HCO_3^- probably due to strong seawater intrusion (data not plotted). The linear coefficients varied between 0.1 and 0.8 for PH and from 0.5 to 0.8 for TO, being the lower values for $K^+-HCO_3^-$ relation and higher for Na^+-HCO_3 and Mg^+-HCO_3. These results support the theory that dissolution from acidic waters is a major mechanism for the mineralization of these groundwaters.

Study of the isotopic signature of dissolved CO_2 ($\delta^{13}C\text{-}CO_2$)

The isotopic composition of dissolved CO_2 ($\delta^{13}C\text{-}CO_2$) gives useful information about the origin of fluids and the chemical and isotopic processes that affect gases during their rise to the surface (Inguaggiato et al., 2000). The $\delta^{13}C\text{-}CO_2$ data present average values of −8.1, −10.9, and −4.7‰ vs. VPDB for PH, TO, and LS, respectively. The temporal evolutions for the three sampling points show two periods where a change to more endogenous values in $\delta^{13}C\text{-}CO_2$ is observed: one after the February 2018 seismic swarm and the second during the eruption (Figure 10). The samples belonging to LS have a more endogenous carbon signature with respect to those from PH and TO. This could be explained because LS is in the southern part of La Palma (Figure 1) where the Teneguía eruption (1971) occurred, so despite having a strong marine intrusion, it is an excellent point for volcano monitoring. A zoom of the plotted data is shown in Figure 10B in which the increasing trend to more endogenous values in the three sampling points is remarkable during the eruption as a consequence of an increase in the dissolved volcanic origin CO_2. Considering that the typical values of $\delta^{13}C\text{-}CO_2$ in the MORB source are in the range -8‰ -5‰ (Sano and Marty, 1995), higher values of $\delta^{13}C\text{-}CO_2$

derive from the thermal decomposition of marine carbonates and lower values correspond to CO_2 degassed from the mantle (Grassa et al., 2006). These changes in $\delta^{13}C\text{-}CO_2$ were also observed in the soil gas CO_2 measured in the continuous mode with an isotope ratio infrared spectrometer (Asensio-Ramos et al., 2022). An increasing trend of fewer negative values was detected from the beginning of 2021 to the moment when the eruption started, showing an increasing magmatic component in the soil CO_2 measured. This change is attributed to the increasing output of deep gases likely produced by the depressurization of a rising batch of deep gas-rich magma (Carapezza et al., 2004).

Conclusion

This hydrogeochemical study of the groundwaters from PH and TO galleries and the LS well has enabled a better understanding of the impact of the input of magmatic fluids on the volcanic system before and during the 2021 Tajogaite eruption.

The groundwaters from PH and TO are of $Na^+-K^+-HCO_3^-$ type, while those from LS are a Na^+-Cl^- type due to seawater intrusion. pH and EC values show significant changes directly related to acid volcanic gases' (HCl, H_2S, SO_2, HF, etc.) dissolution, as a consequence of different seismic swarms and the eruption which occurred in September 2021. The occurrence of seismic swarms perturbed the magmatic reservoir, and hydrothermal volcanic gases (mainly CO_2) were released, while during the eruptive period, large quantities of gases were emitted. Both cases involve gas emissions, of which one portion is released into the atmosphere and another can be trapped or dissolved in the aquifer. These processes also affected the total alkalinity (HCO_3^- content) and anion concentrations (F^-, Cl^-, Br^-, and SO_4^{2-}). In addition, the isotopic values of $\delta^{13}C\text{-}CO_2$ confirm the interaction of groundwaters with deep fluids, showing an interesting change to more endogenous values during the eruptive period.

This study demonstrates the suitability of monitoring the chemical and isotopic composition of groundwaters as they are sensitive to changes in volcanic activity. These studies play a fundamental role as a complement to other geochemical studies of the visible manifestations of volcanic fluid discharges or diffuse degassing in volcanic areas.

Data availability statement

The original contributions presented in the study are included in the article/Supplementary Material; further inquiries can be directed to the corresponding author.

Author contributions

CA, MA, and GM contributed to the conception and design of the study. CA organized the database, performed field and laboratory work, reprocessed all the data, created and edited the figures, and wrote the first draft of the manuscript. CA and GM performed the statistical analysis. MA-R and GM made all the revisions to the manuscript. All authors contributed to the manuscript revision and read and approved the submitted version.

Funding

Acknowledgments

Conflict of interest

The authors declare that the research was conducted in the absence of any commercial or financial relationships that could be construed as a potential conflict of interest.

Publisher's note

All claims expressed in this article are solely those of the authors and do not necessarily represent those of their affiliated organizations, or those of the publisher, the editors, and the reviewers. Any product that may be evaluated in this article, or claim that may be made by its manufacturer, is not guaranteed or endorsed by the publisher.

Supplementary material

The Supplementary Material for this article can be found online at: https://www.frontiersin.org/articles/10.3389/feart.2022.1003890/full#supplementary-material

References

Agencia Estatal de Meteorología (AEMET) (2022). *Agencia Estatal de Meteorología*. Available at: https://www.aemet.es/es/serviciosclimaticos/vigilanciaclima/analisis_estacional?w=1&l=C139E&datos=prec.

Aiuppa, A., Federico, C., Franco, A., Giudice, G., Gurrieri, S., Inguaggiato, S., et al. (2005). Emission of bromine and iodine from Mount Etna volcano. *Geochem. Geophys. Geosyst.* 6. doi:10.1029/2005GC000965

Alcalá, F., and Custodio, M. (2008). Using the Cl/Br ratio as a tracer to identify the origin of salinity in aquifers in Spain and Portugal. *J. Hydrology.* 359, 189–207. doi:10.1016/j.jhydrol.2008.06.028

Allard, P., Carbonelle, J., Dajlevic, D., Le Bronec, J., Morel, P., Robe, M. C., et al. (1991). Eruptive and diffuse emissions of CO_2 from mount Etna. *Nature* 351, 387–391. doi:10.1038/351387a0

Allard, P., Jean-Baptiste, P., D´Alessandro, W., Parello, F., Parisi, B., and Flechoc, C. (1997). Mantle-derived helium and carbon in groundwaters and gases of Mount Etna, Italy. *Earth Planet. Sci. Lett.* 148, 501–516. doi:10.1016/s0012-821x(97)00052-6

Alonso, M., Pérez, N., Padrón, E., Hernández, P., Melián, G., Sumino, H., et al. (2021). Changes in the thermal energy and the diffuse ^{3}He and ^{4}He degassing prior to the 2014–2015 eruption of Pico do Fogo volcano, Cape Verde. *J. Volcanol. Geotherm. Res.* 416, 107271. doi:10.1016/j.jvolgeores.2021.107271

Amonte, C., Asensio-Ramos, M., Melián, G. V., Pérez, N. M., Padrón, E., Hernández, P. A., et al. (2021). Hydrogeochemical temporal variations related to changes of seismic activity at Tenerife, Canary Islands. *Bull. Volcanol.* 83, 24. doi:10.1007/s00445-021-01445-4

Amonte, C., Pérez, N. M., Melián, G. V., Asensio-Ramos, M., Padrón, E., and Hernández, P. A. (2022). Temporal evolution of dissolved gases in groundwater of Tenerife Island. *J. Volcanol. Geotherm. Res.* 424, 107512. doi:10.1016/j.jvolgeores.2022.107512

Ancochea, E., Hernán, F., Cendrero, A., Cantragrel, J. M., Fúster, J. M., Ibarrola, E., et al. (1994). Constructive and destructive episodes in the building of a young oceanic island, La Palma, canary islands, and Genesis of the caldera de Taburiente. *J. Volcanol. Geotherm. Res.* 60, 243–262. doi:10.1016/0377-0273(94)90054-x

Armienta, M. A., De la Cruz-Reyna, S., Gómez, A., Ramos, E., Ceniceros, N., Cruz, O., et al. (2008). Hydrogeochemical indicators of the Popocatépetl volcano activity. *J. Volcanol. Geotherm. Res.* 170, 35–50. doi:10.1016/j.jvolgeores.2007.09.006

Asensio-Ramos, M., Padrón, E., Barrancos, J., Hernández, P. A., Melián, G. V., Rodríguez, F., et al. (2022). *Continuous measurement of carbon isotopic composition in soil gases at Cumbre Vieja volcano: A new challenge in volcano monitoring*. Viena: European Geosciences Union Meeting.

Bellia, C., Gallardo, A., Yasuhara, M., and Kazahaya, K. (2015). Geochemical characterization of groundwater in a volcanic system. *Resources* 4, 358–377. doi:10.3390/resources4020358

Benavides, A. (2019). La hidrogeología del entorno del Parque Nacional de la Caldera de Taburiente, La Palma (Islas Canarias). *Bol. Geol. Min.* 130, 641–660. doi:10.21701/bolgeomin.130.4.004

Bravo, T., and Coello, J. (1979). *Contribución a la hidrogeología de la Caldera de Taburiente, La Palma, Islas Canarias. II Simposio Nacional de Hidrogeología*. Pamplona, 525–532.

Burton, M., Allard, P., Muré, F., and Oppenheimer, C. (2003). FTIR remote sensing of fractional magma degassing at Mt. Etna, Sicily, In: Volcanic degassing. *Geol. Soc. Lond. Spec.Publ.* 213, 281–293. doi:10.1144/gsl.sp.2003.213.01.17

Capasso, G., and Inguaggiato, S. (1998). A simple method for the determination of dissolved gases in natural waters. An application to thermal waters from Vulcano Island. *Appl Geochem* 13, 631–642

Capasso, G., Favara, R., Francofonte, S., and Inguaggiato, S. (1999). Chemical and isotopic variations in fumarolic discharge and thermal waters at Vulcano island (aeolian islands, Italy) during 1996: Evidence of resumed volcanic activity. *J. Volcanol. Geotherm. Res.* 88, 167–175. doi:10.1016/s0377-0273(98)00111-5

Carapezza, M. L., Inguaggiato, S., Brusca, L., and Longo, M. (2004). Geochemical precursors of the activity of an open-conduit volcano: The Stromboli 2002-2003 eruptive events: Geoph.Res.Letters, 31:L07620. Capasso G, Inguaggiato S, (1998) A simple method for the determination of dissolved

gases in natural waters. An application to thermal waters from Vulcano Island. *Appl. Geochem* 13, 631–642. doi:10.1029/2004GL019614

Chiodini, G., Frondini, F., Kerrick, D. M., Rogie, J., Parello, F., Peruzzi, L., et al. (1999). Quantification of Deep CO_2 fluxes from Central Italy. Examples of carbon balance for regional aquifers and of soil diffuse degassing. *Chem. Geol.* 159, 205–222. doi:10.1016/s0009-2541(99)00030-3

Chiodini, G., Frondini, F., and Raco, B. (1996). Diffuse emission of CO_2 from the fossa crater, Vulcano island (Italy). *Bull. Volcanol.* 58, 41–50. doi:10.1007/s004450050124

Custodio, E. (1986). *Groundwater characteristics and problems in volcanic rock terrains Isotope techniques in the study of hydrology of fractured and fissured rocks Proceedings of an Advisor Group Meeting*. Vienna, Austria: Agencia Internacional de la Energía Atómica Viena.

D'Addabbo, M. (2006). *Human fluorosis related to volcanic activity: A review. Environ. Toxicol.* [10.2495/ETOX060031].

D'Addabbo, M., Sulpizio, R., Guidi, M., Capitani, G., Mantecca, P., and Zanchetta, G. (2015). Ash leachates from some recent eruptions of Mount Etna (Italy) and Popocatépetl (Mexico) volcanoes and their impact on amphibian living freshwater organisms. *Biogeosciences* 12, 7087–7106. doi:10.5194/bg-12-7087-2015

D'Alessandro, W. (2006). Human fluorosis related to volcanic activity: a review. *Environ. Toxicol.* doi:10.2495/ETOX060031

D'Auria, L., Koulakov, I., Prudencio, J., Cabrera-Pérez, I., Ibanez, J., Barrancos, J., et al. (2022). *Voluminous storage and rapid magma ascent beneath La Palma revealed by seismic tomography*. doi:10.21203/rs.3.rs-1238072/v1

Day, S. J., Carracedo, J. C., Guillou, H., and Gravestock, P. (1999). Recent structural evolution of the Cumbre Vieja volcano, canary islands: Volcanic rift zones reconfiguration as a precursor to volcano flank instability? *J. Volcanol. Geotherm. Res.* 94, 135–167. doi:10.1016/s0377-0273(99)00101-8

Federico, C., Aiuppa, A., Allard, P., Bellomo, S., Jean-Baptiste, J., Parello, F., et al. (2002). Magma-derived gas influx and water-rock interactions in the volcanic aquifer of Mt. Vesuvius, Italy. *Geochim. Cosmochim. Acta* 66, 963–981. doi:10.1016/s0016-7037(01)00813-4

Federico, C., Aiuppa, A., Favara, R., Gurrieri, S., and Valenza, M. (2004). Geochemical monitoring of groundwaters (1998-2001) at Vesuvius volcano (Italy). *J. Volcanol. Geotherm. Res.* 133, 81–104. doi:10.1016/s0377-0273(03)00392-5

Gerlach, T. M., Doukas, M. P., McGee, K. A., and Kessler, R. (2001). Soil efflux and total emission rates of magmatic CO2 at the Horseshoe Lake tree kill, Mammoth Mountain, California, 1995–1999. *Chem. Geol.* 177, 101–116. doi:10.1016/s0009-2541(00)00385-5

Grassa, F., Capasso, G., Favara, R., and Inguaggiato, S. (2006). Chemical and isotopic composition of waters and dissolved gases in some thermal springs of sicily and adjacent volcanic islands, Italy. *Pure Appl. Geophys.* 163, 781–807. doi:10.1007/s00024-006-0043-0

Hayer, C., Barrancos, J., Burton, M., Rodríguez, F., Esse, B., Hernández, P., et al. (2022). *From up above to down below: Comparison of satellite- and ground-based observations of SO2 emissions from the 2021 eruption of Cumbre Vieja, La Palma*. Viena: European Geosciences Union Meeting.

Hernández, P. A., Notsu, K., Salazar, J. M., Mori, T., Natale, G., Okada, H., et al. (2001). Carbon dioxide degassing by advective flow from usu volcano, Japan. *Science* 292, 83–86. doi:10.1126/science.1058450

Hernández, P. A., Notsu, K., Okada, H., Mori, T., Sato, M., Barahona, F., et al. (2006). Diffuse emission of CO_2 from showa-shinzan, hokkaido, Japan: A sign of volcanic dome degassing. *Pure Appl. Geophys.* 163, 869–881. doi:10.1007/s00024-006-0038-x

Inguaggiato, S., Diliberto, I. S., Federico, C., Paonita, A., and Vita, F. (2018). Review of the evolution of geochemical monitoring, networks and methodologies applied to the volcanoes of the Aeolian Arc (Italy). *EartH*, 2486. doi:10.1016/j.earscirev.2017.09.006

Inguaggiato, S., Pecoraino, G., and D'Amore, F. (2000). Chemical and isotopical characterisation of fluid manifestations of Ischia Island (Italy). *J. Volcanol. Geotherm. Res.* 99, 151–178. doi:10.1016/s0377-0273(00)00158-x

Inguaggiato, S., Vita, F., Rouwet, D., Bobrowski, N., Morici, S., and Sollami, A. (2011). Geochemical evidence of the renewal of volcanic activity inferred from CO_2 soil and SO_2 plume fluxes: The 2007 Stromboli eruption (Italy). *Bull. Volcanol.* 73, 443–456. doi:10.1007/s00445-010-0442-z

JRC (2021). *volcano eruption in La Palma, Spain (2021-09-19)*. European Commission, Joint Research Centre. Available at: http://data.europa.eu/89h/6fc2d36e-890c-47b8-9f5f-662816238678.

King, C. Y. (1986). Gas geochemistry applied to earthquake prediction: An overview. *J. Geophys. Res.* 91 (B12), 12269–12281. doi:10.1029/jb091ib12p12269

König, B. (1997). *Determination of solute fluxes and balances in the groundwater of the volcanic island of La Palma (Canary Islands)*. Kiel, Germany: Universität.

Marrero, R. (2010). *Modelo Hidrogeoquímico del acuífero de Las Cañadas del Teide Tenerife Islas*. Santa Cruz de Tenerife, Spain: Canarias Universidad Politécnica de Cataluña.

Martin-Del Pozo, A. L., Aceves, F., Espinasa, R., Aguayo, A., Inguaggiato, S., Morales, P., et al. (2002). Influence of volcanic activity on spring water chemistry at Popocatépetl Volcano, Mexico. *Chem. Geol.* 190, 207–229. doi:10.1016/s0009-2541(02)00117-1

Melián, G., Tassi, F., Pérez, N., Hernández, P., Sortino, F., Vaselli, O., et al. (2012). A magmatic source for fumaroles and diffuse degassing from the summit crater of teide volcano (Tenerife, canary islands): A geochemical evidence for the 2004–2005 seismic–volcanic crisis. *Bull. Volcanol.* 74 (6), 1465–1483. doi:10.1007/s00445-012-0613-1

Melián, G., Hernández, P. A., Padrón, E., Pérez, N. M., Barrancos, J., Padilla, G., et al. (2014). Spatial and temporal variations of diffuse CO_2 degassing at El Hierro volcanic system: Relation to the 2011–2012 submarine eruption. *J. Geophys. Res. Solid Earth* 119, 6976–6991. doi:10.1002/2014jb011013

Melián, G., Toulkeridis, T., Pérez, N., Hernández, P., Somoza, L., Padrón, E., et al. (2021). Geochemistry of water and gas emissions from Cuicocha and Quilotoa volcanic lakes, Ecuador. *Front. Earth Sci.* 9, 741528. doi:10.3389/feart.2021.741528

Melián, G., Meire, A., Amonte, C., Pitti, L., Di Nardo, D., Alonso, M., et al. (2022). *Diffuse He and H2 emissions from Cumbre Vieja volcano before and during the recent eruption, La Palma, canary islands*. Viena: European Geosciences Union Meeting.

Mori, T., Hernández, P. A., Salazar, J. M. L., Pérez, N. M., and Notsu, K. (2001). An *in-situ* method for measuring CO_2 flux from volcanic-hydrothermal fumaroles. *Chem. Geol.* 177, 85–99. doi:10.1016/s0009-2541(00)00384-3

Naselli, L., Barone, R., and Mosello, R. (2003). Eutrophication control by lime addition: A preliminary approach in Sicilian reservoirs. *Hydrobiologia* 504, 297–303. doi:10.1023/b:hydr.0000008529.57172.d6

Navarro, J. M. (1993). *Avance del Plan Hidrológico Insular*. Vivienda y Aguas: Consejería de Obras Públicas.

Padrón, E. (2015). *Geoquímica de emanaciones difusas en sistemas volcánicos implicaciones para la exploración geotérmica y la vigilancia volcánica en canarias*. Santa Cruz de Tenerife, Spain: Universidad de La Laguna.

Padrón, E., Melián, G., Marrero, R., Nolasco, D., Barrancos, J., Padilla, G., et al. (2008). "Changes on diffuse CO_2 emission and relation to seismic activity in and around El Hierro, Canary Islands, Spain," in *PAGEOPH topical volume, terrestrial fluids, earthquakes and volcanoes: The hiroshi wakita*, Vol. III. (in press).

Padrón, E., Hernández, P. A., Pérez, N. M., Toulkeridis, T., Melián, G., Barrancos, J., et al. (2012). Fumarole/plume and diffuse CO_2 emission from Sierra Negra caldera, Galapagos archipelago. *Bull. Volcanol.* 74, 1509–1519. doi:10.1007/s00445-012-0610-4

Padrón, E., Pérez, N. M., Rodríguez, F., Melián, G., Hernández, P. A., Hirochika, S., et al. (2015). Dynamics of diffuse carbon dioxide emissions from Cumbre Vieja volcano, La Palma, canary islands. *Bull. Volcanol.* 77, 28–15. doi:10.1007/s00445-015-0914-2

Padrón, E., Pérez, N., Hernández, P., Melián, G., Asensio-Ramos, M., D'Auria, L., et al. (2021). Changes in diffuse degassing from the summit crater of teide volcano (Tenerife, canary islands) prior to the 2016 Tenerife long-period seismic swarm. *J. Geophys. Res. Solid Earth* 126, e2020JB020318. doi:10.1029/2020jb020318

Pankhurst, M. J., Scarrow, J. H., Barbee, O. A., Hickey, J., Coldwell, B. C., Rollinson, G. K., et al. (2022). Rapid response petrology for the opening eruptive phase of the 2021 Cumbre Vieja eruption, La Palma, Canary Islands. *Volcanica* 5 (1), 1–10. doi:10.30909/vol.05.01.0110

Pardo, A., Burton, M., Asensio-Ramos, M., Barrancos, J., La Spina, A., Allard, P., et al. (2002). *Insights into magma degassing processes during the 2021 Cumbre Vieja eruption, La Palma, from open-path FTIR spectroscopy*. Viena: European Geosciences Union Meeting.

Pérez, N. M., Wakita, H., Nakai, S., Sano, Y., and Williams, S. N. (1994). 3He/4He isotopic ratios in volcanic-hydrothermal discharges from the canary islands, Spain: Implications on the origin of the volcanic activity. *Mineral. Mag.* 58A, 709–710. doi:10.1180/minmag.1994.58a.2.107

Pérez, N. M., Hernández, P. A., Padrón, E., Melián, G., Marrero, R., Padilla, G., et al. (2007). Precursory subsurface 222Rn and 220Rn degassing signatures of the 2004 seismic crisis at Tenerife Canary Islands. *Pure Appl. Geophys.* 164, 2431–2448. doi:10.1007/s00024-007-0280-x

Pérez, N. M., Hernández, P. A., Igarashi, G., Trujillo, I., Nakai, S., Sumino, H., et al. (2008). Searching and detecting earthquake geochemical precursors in CO_2-rich groundwaters from Galicia, Spain. *Geochem. J.* 42, 75–83. doi:10.2343/geochemj.42.75

Pérez, N. M., Hernández, P. A., Padrón, E., Melián, G., Nolasco, D., Barrancos, J., et al. (2013). An increasing trend of diffuse CO2 emission from teide volcano (Tenerife, canary islands): Geochemical evidence of magma degassing episodes. *J. Geol. Soc. Lond.* 170 (4), 585–592. doi:10.1144/jgs2012-125

PEVOLCA (2022a). *Special plan for civil protection and emergency attention due to volcanic risk in the Canary Islands (PEVOLCA)*. Report of September 19, 2021 in the afternoon Available at: https://www.gobiernodecanarias.org/cmsweb/export/sites/infovolcanlapalma/galerias/documentos/informes-pevolca/19092021-Tarde-Comite-Cientifico-PEVOLCA.pdf.

PEVOLCA (2022b). *Special plan for civil protection and emergency attention due to volcanic risk in the Canary Islands (PEVOLCA)*. Reports Available at: https://www.gobiernodecanarias.org/infovolcanlapalma/pevolca/.

Rodríguez, F., Pérez, N., Amonte, C., Martín-Lorenzo, A., Melián, G., Codwell, B., et al. (2022). *Geochemistry of ash leachates during the 2021 eruption of Cumbre Vieja volcano, La Palma, canary islands*. Viena: European Geosciences Union Meeting.

Romero, J., Burton, M., Cáceres, F., Taddeucci, J., Civico, R., and Ricci, T. (2022) The initial phase of the 2021 Cumbre Vieja ridge eruption (Canary Islands): Products and dynamics controlling edifice growth and collapse. *J. Volcanol. Geotherm. Res.* 431, 107642.

Rouwet, D., Bellomo, S., Brusca, L., Inguaggiato, S., Jutzeler, M., Mora, R., et al. (2009). Major and trace element geochemistry of El chichón volcano-hydrothermal system (chiapas, méxico) in 2006-2007: Implications for future geochemical monitoring. *GeofInt.* 48, 55–72. doi:10.22201/igeof.00167169p.2009.48.1.99

Salazar, J. M. L., Pérez, N. M., Hernández, P. A., Soriano, T., Barahona, F., Olmos, R., et al. (2002). Precursory diffuse carbon dioxide degassing signature related to a 5.1 magnitude earthquake in El Salvador, Central America. *Earth Planet. Sci. Lett.* 205, 81–89. doi:10.1016/s0012-821x(02)01014-2

Sano, Y., and Marty, B. (1995). Origin of carbon in fumarolic gas from island arcs. *Chem. Geol.* 119, 265–274. doi:10.1016/0009-2541(94)00097-r

Santana de León, J. M., Melián, G., Rodriguez, C., Cervigón-Tomico, G., Ortega, V., Martínez, D., et al. (2022). *Long-term variations of diffuse CO2 at Cumbre Vieja volcano, La Palma, canary islands*. Viena: European Geosciences Union Meeting.

Sinclair, A. J. (1974). Selection of threshold values in geochemical data using probability graphs. *J. Geochem. Explor.* 3, 129–149. doi:10.1016/0375-6742(74)90030-2

Staudigel, H., Feraud, G., and Giannerini, G. (1986). The history of intrusive activity on the island of La Palma (Canary Islands). *J. Volcanol. Geotherm. Res.* 27, 299–322. doi:10.1016/0377-0273(86)90018-1

Taran, Y., Zelenski, M., Chaplygin, I., Malik, N., Campion, R., Inguaggiato, S., et al. (2018). Gas emissions from volcanoes of the kuril island arc (NW pacific): Geochemistry and fluxes. *Geochem. Geophys. Geosyst.* 19, 1859–1880. doi:10.1029/2018GC007477

Thomas, D. (1988). Geochemical precursors to seismic activity. *Pure Appl. Geophys* 126, 241–266. doi:10.1007/bf00878998

Veeger, A. I. (1991). *Geochemical methods for evaluating the origin and evolution of ground water in volcanic rocks at La Palma (Canary Islands, Spain)*. Tucson, AZ: University of Arizona.

Global Volcanism Program (2013). in *La Palma (383010) in volcanoes of the world, v. 4.11.0 (08 jun 2022)*. Editor E. Venzke (Smithsonian Institution). Downloaded available at: https://volcano.si.edu/volcano.cfm?vn=383010.

Wadsworth, F. B., Llewellin, E. W., Farquharson, J. I., Gillies, J. K., Loisel, A., Frey, L., et al. (2022). Crowd-sourcing observations of volcanic eruptions during the 2021 Fagradalsfjall and Cumbre Vieja events. *Nat. Commun.* 13, 2611. doi:10.1038/s41467-022-30333-4

Wakita, H., Fuji, N., Matsuo, S., Notsu, K., Nagao, K., and Takaoka, N. (1978). Helium spots": Caused by a diapiric magma from the upper mantle. *Science* 200, 430–432. doi:10.1126/science.200.4340.430

Zhang, J., Quay, P. D., and Wilbur, D. O. (1995). Carbon isotope fractionation during gas-water exchange and dissolution of CO_2. *Geochim. Cosmochim. Acta* 59, 107–114. doi:10.1016/0016-7037(95)91550-d

Zheng, Z., Fu, Y., Liu, K., Xiao, R., Wang, X., and Shi, H. (2018). Three-stage vertical distribution of seawater conductivity. *Sci. Rep.* 8, 9916. doi:10.1038/s41598-018-27931-y